NMR Analysis of the Transient Complex between Membrane Photosystem I and Soluble Cytochrome c_6*[S]

Irene Díaz-Moreno‡, Antonio Díaz-Quintana‡, Fernando P. Molina-Heredia‡, Pedro M. Nieto§, Örjan Hansson¶, Miguel A. De la Rosa‡‖, and B. Göran Karlsson**‡‡

*From the ‡Instituto de Bioquímica Vegetal y Fotosíntesis and the §Instituto de Investigaciones Químicas, Universidad de Sevilla y Consejo Superior de Investigaciones Científicas, Américo Vespucio 49, 41092 Sevilla, Spain, ¶Biochemistry and Biophysics, Department of Chemistry, Göteborg University, 405 30 Göteborg, Sweden, the **Department of Chemistry and Bioscience, Chalmers University of Technology, Box 462, 405 30 Göteborg, Sweden, and the ‡‡Swedish NMR Centre, Hasselblad Laboratory, Göteborg University, Box 465, 405 30 Göteborg, Sweden*

A structural analysis of the surface areas of cytochrome c_6, responsible for the transient interaction with photosystem I, was performed by NMR transverse relaxation-optimized spectroscopy. The hemeprotein was titrated by adding increasing amounts of the chlorophyllic photosystem, and the NMR spectra of the free and bound protein were analyzed in a comparative way. The NMR signals of cytochrome c_6 residues located at the hydrophobic and electrostatic patches, which both surround the heme cleft, were specifically modified by binding. The backbones of internal residues close to the hydrophobic patch of cytochrome c_6 were also affected, a fact that is ascribed to the conformational changes taking place inside the hemeprotein when interacting with photosystem I. To the best of our knowledge, this is the first structural analysis by NMR spectroscopy of a transient complex between soluble and membrane proteins.

NMR spectroscopy makes it possible to observe the signals of particular atoms in the free and bound states of any molecule (1) and has thus become an essential tool for the analysis of protein-protein interactions (2). Depending on both the time scale of the relaxation process and the exchange kinetics, the NMR signals of the free protein can provide relevant information on its bound state.

Conventional solution NMR spectroscopy is usually limited to complexes with a molecular mass lower than 50 kDa because of their quick tumbling, and it relies on the average of orientation-dependent dipolar interactions and chemical shifts. Slow tumbling makes the structural analysis of membrane-attached proteins difficult because of the large size of lipid bilayers. It is possible to study the membrane complexes in uniaxially oriented samples, although another alternative is to use solid state NMR, in which transverse relaxation is minimized by eliminating its two components, the chemical shift anisotropy and the dipolar coupling between paramagnetic nuclei (3).

Most of the current experimental data in the literature concern the interaction between a small soluble molecule (*e.g.* drug) and the extracellular domains of a membrane protein (4). The structure of small signaling peptides when bound to their specific membrane receptors has also been analyzed, and the conformation of the receptor-bound form of a 27-residue peptide has been determined by transferred nuclear Overhauser effect upon digitonin solubilization of the membrane receptor (5). These techniques, which have not been employed yet with large protein complexes, are probably not useful for the study of transient protein-protein interactions.

Transverse relaxation-optimized spectroscopy (TROSY),[1] which is based on the mutual cancellation between chemical shift anisotropy and dipolar coupling contributions at high fields (6), has already been used to analyze slowly tumbling molecules (7). It has also been used in the structural analysis of protein-protein interactions within large systems, namely the 900-kDa GroEL-GroES complex (8) and the tumor suppressor p53 upon binding to Hsp90 (9).

We have thus employed such detection techniques, along with adequate isotopic labeling, to study the interaction areas within the physiological transient complex formed by a large membrane complex and a small soluble protein. In particular, we look at the 1-MDa membrane-embedded photosystem I (PSI) reaction center and its 10-kDa electron donor protein cytochrome c_6. This is an excellent model system to validate our novel experimental approach, as there is a large amount of structural and functional data in the literature for both the chlorophyllic complex and the metalloprotein from a wide variety of organisms (10, 11). In cyanobacteria, the functional interaction between PSI and cytochrome c_6 has been investigated extensively by using time-resolved optical spectroscopy and site-directed mutagenesis (see Ref. 12 for a review). In cytochrome c_6, two functional areas have been identified: a hydrophobic patch for electron transfer (site 1) and an electrically charged area for complex formation (site 2). In PSI, the H loop of its PsaB subunit seems to be involved in electrostatic interactions with the electron donor (13, 14), whereas a tryptophan dimer at the i/j loops of PsaA/B could be responsible for the hydrophobic interactions at the recognition site.

In this work, we investigated the residues of cytochrome c_6 involved in the interaction with PSI by using TROSY NMR spectroscopy. To our knowledge, this is the first NMR analysis

[1] The abbreviations used are: TROSY, transverse relaxation-optimized spectroscopy; PSI, photosystem I.

of the residues of a soluble protein involved in the interaction with a large membrane complex.

EXPERIMENTAL PROCEDURES

Protein Preparation—Uniformly ^{15}N-labeled cytochrome c_6 from the cyanobacterium *Nostoc sp.* PCC 7119 was produced in *Escherichia coli* JM109 cells transformed with the pEAC-WT (15) and pEC86 (16) plasmids. Culture conditions and protein purification methods were as described previously (17).

Trimeric PSI particles were obtained as described by Hervás *et al.* (18), and PSI monomers were purified by following the same method but replacing calcium salt with 200 mM $MgCl_2$ (19). The thylakoidal membranes were treated with 0.2% (w/v) β-dodecylmaltoside for 10 min in the dark. A sucrose gradient ranging from 16 to 22% (w/v) was used to separate PSI from PSII and phycobiliproteins. The P700 content of PSI samples was calculated by following the photoinduced absorbance change at 820 nm and using an absorption coefficient of 6.5 mM^{-1} cm^{-1} (20). Chlorophyll concentration was determined according to Arnon (21).

The PSI preparations were tested by time-resolved optical spectroscopy as described previously (18, 22). The kinetics of P700$^+$ reduction by either plastocyanin or cytochrome c_6 were similar with both PSI trimers and monomers. The data from SDS-PAGE indicated that no PSI subunits were lost during the treatment to get the photosynthetic monomers. An electrophoretic analysis of PSI samples under semi-denatured conditions was routinely performed to check their trimeric or monomeric nature and homogeneity.

NMR Samples—Samples containing either 1.6 mM ^{15}N-labeled cytochrome c_6 or 1.3 mM unlabeled cytochrome c_6 were prepared in 0.3 ml of 95:5 (v/v) H_2O/D_2O solutions containing 10 mM sodium phosphate buffer, pH 6, and 2 mM sodium ascorbate. The cytochrome c_6 samples were concentrated by ultrafiltration (Amicon, YM3 membrane), and their protein concentration was determined spectrophotometrically using an absorption coefficient of 26.2 mM^{-1} cm^{-1} at 553 nm for the ferrous form of cytochrome c_6 (23).

PSI monomers were concentrated using a Vivaspin 2 ml concentrator with a 100-kDa molecular mass cutoff. The buffer used was 10 mM sodium phosphate, pH 6, in 95:5 (v/v) H_2O/D_2O supplemented with 0.025% (w/v) β-dodecylmaltoside. Two different samples were prepared; one had a PSI concentration of 1.80 mM and a chlorophyll/P700 ratio of ~80, and the other had a PSI concentration of 1.08 mM and a chlorophyll/P700 ratio of ~110.

To investigate complex formations between cytochrome c_6 and PSI monomers by NMR, a 0.23-mM ^{15}N-labeled cytochrome c_6 sample was titrated by adding microliter aliquots of a 1.80 or 1.08 mM PSI stock solution. The pH value was adjusted before and after each addition. A sample of free cytochrome c_6 in the same buffer (10 mM sodium phosphate, pH 6, in 5% (v/v) D_2O solution supplemented with 2 mM sodium ascorbate and 0.025% β-dodecylmaltoside) was used as a reference. Titrations with PSI trimers were performed in a similar way but using a stock solution of 0.2 mM trimeric PSI.

The effect of ionic strength was investigated at pH 6 upon the addition of sodium chloride at varying concentrations. The two-dimensional ^{1}H-^{15}N TROSY spectra (see below) for cytochrome c_6-PSI samples were recorded at 0, 2.5, 5, 10, 20, 40, and 80 mM salt concentration. In all experiments, control measurements were recorded for free cytochrome c_6 under the same conditions.

NMR Spectroscopy—The spectral analysis of the cytochrome c_6-PSI complex was performed on a Varian INOVA 800 NMR spectrometer at 298 K. The two-dimensional ^{1}H-^{15}N TROSY spectra were recorded using spectral widths of 12 ppm (^{1}H) and 30 ppm (^{15}N) as a matrix of 2048×512 complex points. Varian software (VNMR) was employed for spectral processing using zero filling with np(^{1}H) = 4096, ni1(^{15}N) = 1024, and a sine-square window function. A polynomial base-line correction was made automatically.

The analysis of line-broadening perturbations of the PSI-bound hemeprotein with respect to free cytochrome c_6 was performed in SPARKY 3.[2] The sequential assignment of cytochrome c_6 has been reported previously (17). To estimate line widths, the peaks were fitted to a Lorentzian function for the ^{15}N and ^{1}H dimensions. Base-line correction was not performed, and data above the lowest contour level were used to obtain the line widths. Close peaks (less than 100 Hz in ^{15}N and 10 Hz in ^{1}H) were grouped together. A minimization with

10,000 steps and a tolerance of 0.01% was done to fit every signal of the protein backbone.

Four different threshold levels were used for each spectrum to minimize the possible error in line width calculations. Each value was compared with the data inferred from the other three contour levels, and it was rejected when the difference was higher than 4-fold the standard deviation. When the three values were identical and, consequently, the standard deviation was zero, the line width of the analyzed peak was only rejected when the difference with respect to the other three measurements was larger than 5 Hz. Thus, the line width of a signal corresponds to the arithmetic mean of the reliable data according to such criteria.

NMR Line Width Analysis—In the analysis of the line width data ($\Delta\nu_{1/2}$), the overall broadening ($\Delta\Delta\nu_{1/2}$) obtained from signals displaying only minor line broadening was first subtracted from the line width of the corresponding signal. Then, for each residue, the differences of line widths between free and interacting cytochrome c_6 were calculated for each point of the titration series ($\Delta\Delta\nu_{1/2\ \text{Binding}}$). The threshold value, used to identify a specifically broadened residue when data from the titration series were analyzed together, was defined as the average normalized $\Delta\Delta\nu_{1/2\ \text{Binding}}$ for the system plus 2 standard deviations ($2S_{n-1}$). The average $\Delta\Delta\nu_{1/2\ \text{Binding}}$ and the standard deviation were calculated for all amides with normalized values ≤20 Hz on the basis that normalized data >20 Hz clearly indicate a specifically broadened residue and that their inclusion would bias the average to a higher value.

Nostoc Cytochrome c_6 Homology Model—A homology structural model for cytochrome c_6 was built using the COMPOSER module of SYBYL 6.5 (Tripos Inc.) along with the crystal structures for the hemeprotein from *Monoraphidium* (PDB code 1CTJ) (24) and *Chlamydomonas* (PDB code 1CYJ) (25) as templates (26).

RESULTS

Titration of ^{15}N-Labeled Cytochrome c_6 with PSI Monomers—The interaction between cytochrome c_6 and PSI was inferred from the NMR spectra of a ^{15}N-labeled cytochrome c_6 sample recorded upon the addition of increasing amounts of PSI. Only very small chemical shift changes were observed for the cytochrome c_6 signals upon titration. Therefore, the peak assignment in the presence of PSI was obtained by a comparison with the spectrum of free cytochrome c_6. However, the two-dimensional ^{1}H-^{15}N TROSY spectra of cytochrome c_6 before and after the addition of PSI revealed distinct changes in the line width of the signals that can be ascribed to its interaction with PSI. Several signals experienced a broadening significantly larger than the average (Fig. 1*A*), others showed a broadening below the threshold (Fig. 1*B*), and a few signals were in coalescence (Fig. 1*C*). In addition, a set of minor signals appeared immediately adjacent to the existing peaks (Fig. 1*D*).

The histograms in Fig. 2 show the statistical distribution of absolute line width changes ($\Delta\nu_{1/2}$) upon increasing the [PSI]/[cytochrome c_6] ratio. The general line broadening of cytochrome c_6 signals in the ^{15}N and ^{1}H dimensions can be ascribed to the increase in effective molecular mass and concomitant increase in the rotational correlation time of cytochrome c_6 when interacting with PSI. In fact, the effective molecular mass of the complex between cytochrome c_6 and monomeric PSI is ~350 kDa, as compared with the 10-kDa mass of free cytochrome c_6. Such a signal broadening becomes significant at a [PSI](μM)/[cytochrome c_6](μM) ratio of 38/208. It is noteworthy that the indirect (^{15}N) dimension seems to be more sensitive to changes in line widths than the direct (^{1}H) dimension; for the second point of the titration (Fig. 2*C*), the line width distribution is wider, and its maximum shifts to higher values.

In addition to the general line broadening, several amino acidic residues undergo additional changes in ^{15}N and ^{1}H line widths. After normalizing the data (see "Experimental Procedures") and calculating the differences in signal line widths ($\Delta\Delta\nu_{1/2\ \text{Binding}}$) for each titration point (bound cytochrome c_6) and reference (free cytochrome c_6), the backbone amide NMR signals of 26 amino acids of cytochrome c_6 show significant

---

[2] T. D. Goddard and D. G. Kneller, SPARKY 3, University of California, San Francisco.
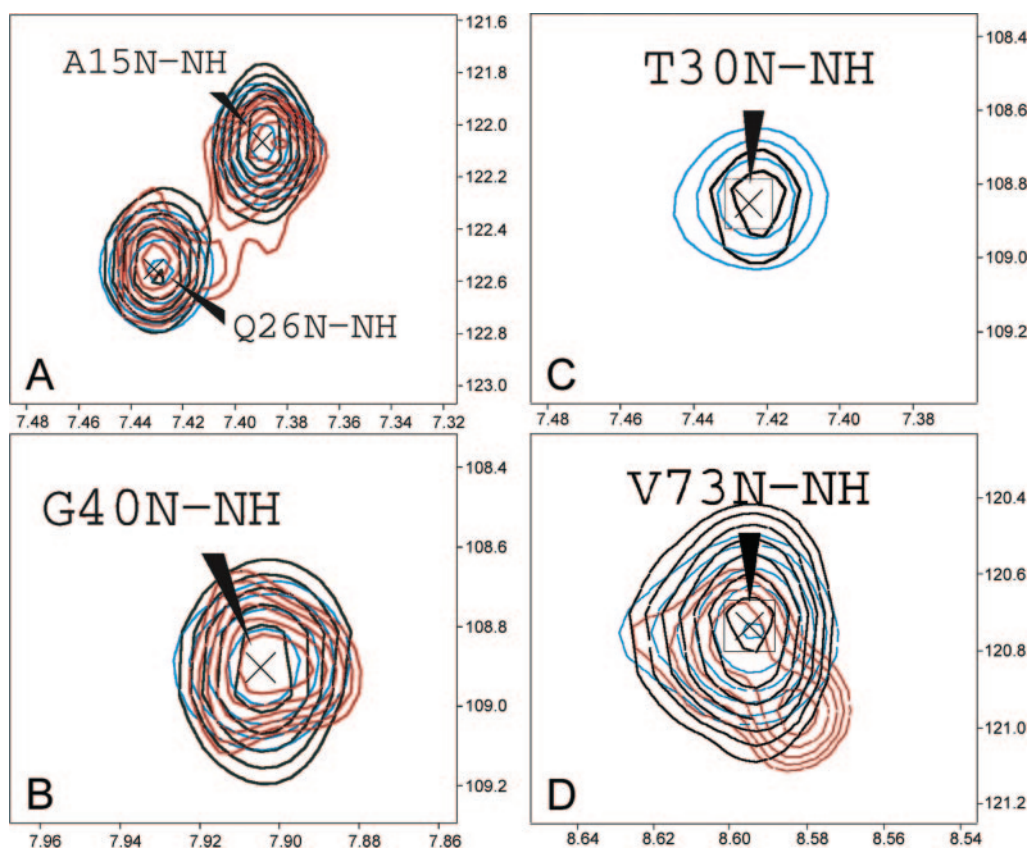
FIG. 1. **Regions from overlaid ^{1}H-^{15}N TROSY spectra of free and PSI-bound *Nostoc* cytochrome c_6.** The [PSI](μM)/[cytochrome c_6](μM) ratios were 0 (*blue*), 38/208 (*black*), and 98/196 (*red*). *A* and *B*, line broadening peaks over and below the threshold value, respectively. *C*, peak in coalescence. *D*, appearance of a minor signal.

changes ($\Delta\Delta\nu_{1/2 \text{ Binding}} \geq \langle\Delta\Delta\nu_{1/2 \text{ Binding}}\rangle + 2S_{n-1}$) in ^{15}N and/or ^{1}H line widths. As shown in Fig. 3, these residues are found in four stretches in the amino acid sequence of cytochrome c_6. The first stretch comprises the residues between positions 9 and 19 (except His-18), and the second stretch comprises the residues between positions 23 and 29. These residues, which belong to site 1 of cytochrome c_6 (12, 26, 27), undergo a specific line width perturbation, with $\Delta\Delta\nu_{1/2 \text{ Binding}} \geq 20$ Hz (^{15}N) and/or ≥ 24 Hz (^{1}H). Some of the signals (*e.g.* Ser-16, Gly-20, and Thr-30) become broadened beyond detection limit throughout the titration process. The third stretch comprises the residues between positions 57 and 66, and the fourth stretch comprises the residues between positions 72 and 79. Proline residues are at positions 59 and 67. Affected residues in these stretches undergo specific $\Delta\Delta\nu_{1/2 \text{ Binding}}$ changes, and some of them (*e.g.* Gly-63) are broadened beyond detection, as are those in the first two stretches.

The residues Lys-62, Arg-64, and Lys-66 are at the electrostatic patch (site 2) of cytochrome c_6 (12, 26, 27). A minor signal appears immediately adjacent to the signals of residues in the third and fourth stretches (*e.g.* residues Ala-57, Met-58, Ala-60, Phe-61, Lys-62, Leu-65, Lys-66, Val-73, Ala-74, and Val-77). The peak displacement of the major signals varies between 0 and 0.08 ppm in the ^{1}H dimension and between 0 and 0.8 ppm in the ^{15}N dimension (Table IS in the supplemental materials). We can exclude the possibility that the new peaks that appear upon PSI addition originate from a bad cancellation of multiple components because the differences in frequencies for most of them do not fall within the range of 85–100 Hz, as would be expected. The new peaks could arise from protein denaturation, but this possibility can also be excluded because a control spectrum with a fresh sample at the maximum PSI concentration displayed similar side peaks. A plausible explanation is

that the peaks are because of the bound form of cytochrome c_6 in slow exchange with the free form. From the observed chemical shift changes, one can then estimate that the rate constant for complex dissociation (k_{off}) is between 1 and 10 s^{-1}. In fact, a k_{off} value of 1.5 s^{-1} and a dissociation constant (K_D) of 9 μM (23) allow an acceptable fit between simulated and experimental line shapes (Fig. 1S in the supplemental materials).

Map of Cytochrome c_6 Residues at the Interface with PSI— The mapping in Fig. 4 shows the residues at the cytochrome c_6 surface (modeled as described under "Experimental Procedures") that are affected by PSI addition, with each residue being colored according to its line broadening in the ^{15}N dimension. Three of the four sequential stretches of residues (Fig. 3) form two main clusters surrounding the heme cleft at the protein surface, and the fourth stretch is located near the first stretch inside the protein. Thus the structural clustering of stretches with broadened residues in cytochrome c_6 suggests that such residues are forming part of two surface areas for interaction with PSI.

Apart from the two patches that define the complex interface, the residues Asp-72, Ala-74, Tyr-76, Leu-78, and Gly-79 on the rear of the protein are also affected (Fig. 4). They belong to the fourth stretch, which is formed by backbone amides (Asp-72, Val-73, Ala-74, Tyr-76, Ala-77, Leu-78, and Gly-79) from helix IV (Fig. 5). These residues, except Asp-72, undergo line width perturbations larger than 4 Hz over the threshold in one or two dimensions. As helix IV is adjacent to some residues of helix I (Ile-9, Phe-10, and Ser-11), the observed changes are probably a secondary effect caused by helix I perturbation.

Electrostatic Effects— The complex between cytochrome c_6 and PSI at a [PSI](μM)/[cytochrome c_6](μM) ratio of 38/208 was investigated in solutions containing 0, 2.5, 5, 10, 20, 40, and 80 mM NaCl (data not shown). The $\Delta\Delta\nu_{1/2 \text{ Binding}}$ values for most
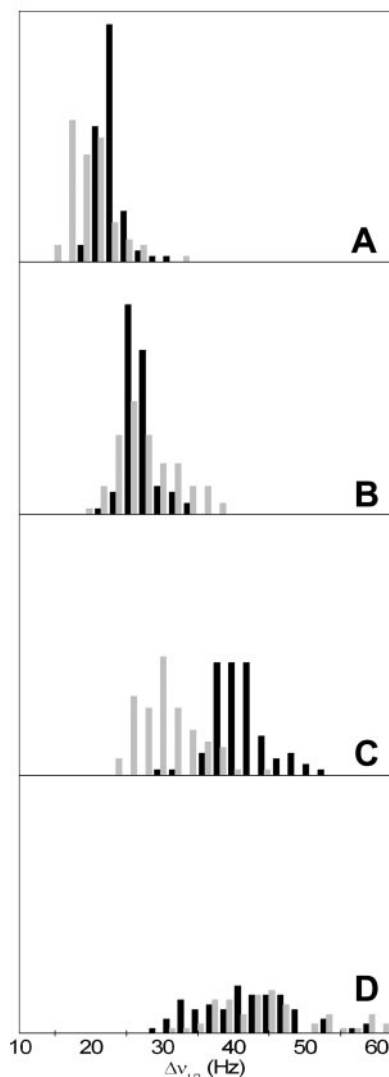
Photosystem I-Cytochrome c₆ Transient Complex

FIG. 2. **Frequency distribution of ^{15}N (*black*) and ^{1}H (*gray*) line widths ($\Delta\nu_{1/2}$) of free and PSI-bound *Nostoc* cytochrome c_6.** Histograms are shown for the following [PSI](μM)/[cytochrome c_6](μM) ratios: 0 (*A*), 18/219 (*B*), 38/208 (*C*), and 98/196 (*D*).

residues decreased with increasing salt concentration, a finding that agrees with the kinetic data reported in the literature (12, 22, 23, 26). Such a decrease in binding affinity reflects the electrostatic nature of the cytochrome c_6-PSI complex. The most strongly affected residues (*e.g.* Glu-37, Lys-62, Lys-66, and Glu-68) undergo a significant signal shift at 40 and 80 mM NaCl. This result is indicative of a strong electrostatic interaction between such charged residues and salt ions. At the highest salt concentration (80 mM), there still remains an ~5-Hz broadening that can be ascribed to the salt effects on the magnetic field homogeneity.

Titration of ^{15}N-Labeled Cytochrome c_6 with PSI Trimers— The molecular mass of the *in vivo* complex between trimeric PSI, which is the physiological form (19), and cytochrome c_6 is >1 MDa. The NMR spectrum of cytochrome c_6 after the addition of PSI trimers is thus weaker than that of the free molecule, although most of the signals can still be observed. A number of spectral signals as high as 29 completely disappear upon binding to PSI (Fig. 6), with a set (Phe-10, Ser-11, Ala-12, Ala-15, Ser-16, Cys-17, His-18, Gly-21, Asn-23, Val-25, Gln-26, Ala-27, Lys-29, and Thr-30) mapping at site 1 of cytochrome c_6. Many of these residues also show a significant broadening upon binding to monomeric PSI.

Other fading peaks correspond to Lys-33, Leu-36, and Met-41, as well as to residues at site 2 (Ala-57, Phe-61, and Lys-62) and helix IV (Leu-78 and Gly-79). The residues Met-58, Lys-66, and Val-73 exhibit a small chemical shift perturbation. PSI trimers and monomers thus induce similar changes on the NMR signals of cytochrome c_6 residues. Such a finding indicates that the same regions of cytochrome c_6 are involved in the interaction with both trimeric and monomeric PSI.

DISCUSSION

The Cytochrome c_6-PSI Interaction—The interaction between cytochrome c_6 and PSI is studied herein by using both the monomeric (Fig. 1) and trimeric (Fig. 6) forms of PSI. Upon titration of cytochrome c_6 with increasing amounts of PSI, no fast chemical exchange is observed within the spectral time scale, but the corresponding global and specific line broadenings are indicative of changes in the apparent transversal relaxation time. This finding, along with the appearance of distinct side peaks, suggests the occurrence of a slow chemical exchange. In such an exchange regime, the broadening of free cytochrome c_6 signals would be because of the contribution of the complex to the transverse relaxation rate, yielding information on the dynamics of cytochrome c_6 within the transient complex with PSI. A general line broadening, because of the increase of the global correlation time of the aggregate, is observed for all the signals. Simultaneously, we can detect specific changes that can be ascribed to differences in local internal motions upon interaction with PSI. Some other phenomena could contribute to the line broadening of signals (*e.g.* Ser-16, Gly-20, Thr-30, and Gly-63) beyond detection limits. Recently, several studies (28, 29) show that the interaction sites often suffer a decrease in flexibility because of binding, although the line width could also be influenced by side chain dynamics (30). It is noteworthy that all the fading signals correspond to amino acids with short side chains.

Previous site-directed mutagenesis and kinetic studies had shown that *Nostoc* cytochrome c_6 possesses two functional sites (one hydrophobic (site 1), the other positively charged (site 2), both flanking the heme cleft) for the redox interaction with PSI (12, 26, 27). Such sites perfectly match the two interaction areas herein identified by NMR (Fig. 4).

Binding of cytochrome c_6 to PSI induces changes not only in surface residues but also in some internal residues, namely those at the crossing region between helices I and IV (Fig. 5). As α-helices behave as rigid bodies because of their stabilizing HN_{n+4}–O_n H-bonds, we can assume that the structural changes in helix I upon binding to PSI could transmit the conformational perturbation to neighbor residues in helix IV.

The Binding Model—As the line broadening of residues at site 2 of cytochrome c_6 is smaller than that of amino acids at site 1, we could assume that site 1 is just at the center of the interface area within the transient complex, whereas site 2 is at the interface edge. This would be in agreement with a binding model where the encounter complex is first driven by electrostatic attractions and further stabilized by hydrophobic interactions, as suggested for other electron-transfer complexes (31). In the particular case of *Nostoc*, it is still under debate whether the cytochrome c_6-PSI complex undergoes a "rearrangement step" prior to electron transfer (12, 22, 26, 32). Here we observed that all NMR signals were under slow exchange, and so a kinetically stable intermediate complex could be proposed. Such a long living complex could explain the biphasic kinetics reported for PSI reduction by cytochrome c_6 in flash experiments, thereby making a specific rearrangement step unnecessary (22).

Recent γ-ray-perturbed angular correlation studies have shown a low correlation time (τ_c, ~130 ns) for plastocyanin

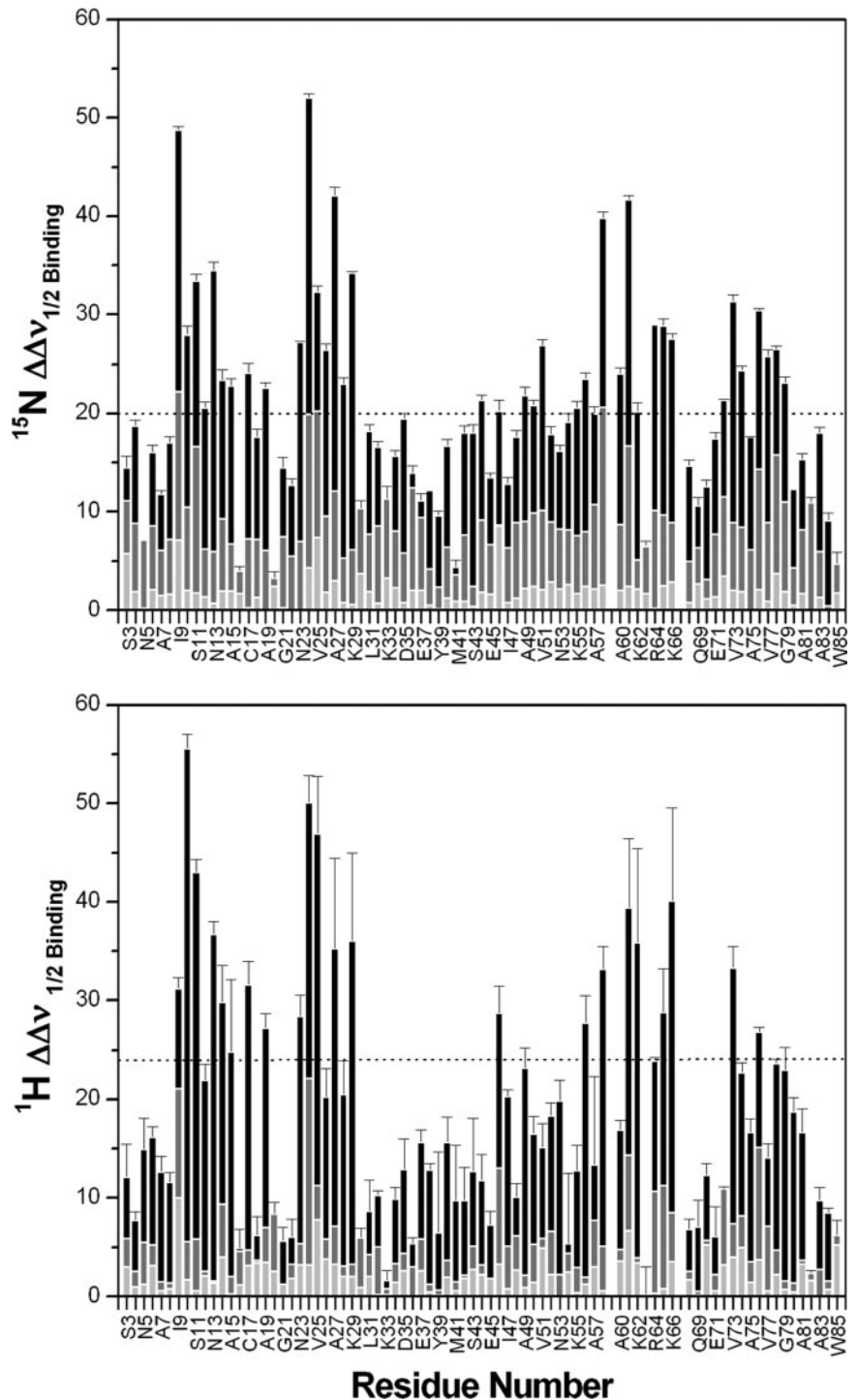FIG. 3. **^{15}N and ^{1}H line width differences ($\Delta\Delta\nu_{1/2\ \text{Binding}}$) between free and PSI-bound *Nostoc* cytochrome c_6.** The data correspond to differences in bandwidth between the NMR spectrum of bound cytochrome c_6 (at the same [PSI]/[cytochrome c_6] ratios as in Fig. 2, *B* (*gray*), *C* (*dark gray*), and *D* (*black*)) and the reference spectrum of the free hemeprotein. The *broken line* on the charts stands for the threshold value, which was calculated as described under "Experimental Procedures."

bound to plant PSI (33) compared with that expected (440 ns) from the molecular weight of the complex. If this would be extrapolated as such to the cytochrome c_6-PSI complex, the amides at the interface edge of the bound hemeprotein would not be totally frozen, and their NMR signals could still remain detectable in the complex (a non-symmetrical two-site exchange simulation is available as supplemental data).

We have recently analyzed the interaction of *Nostoc* cytochrome c_6 with soluble cytochrome *f* from *Phormidium laminosum* (17). The calculated K_D value for this complex ($\sim$100 μM) is higher than that reported for the interaction of *Nostoc* cytochrome c_6 with PSI ($\sim$9 μM) (23). Such a difference of 1 order of magnitude in their respective K_D values could be indicative of two different types of exchanges for cytochrome c_6 (one fast

with cytochrome *f*, the other slow with PSI), although it exploits the same surface areas for the interactions with its two membrane partners. Formation of the cytochrome c_6-PSI complex strongly depends on ionic strength, but such an ionic dependence is probably not the only factor explaining the large differences in exchange regime and lifetime between the two transient complexes. Also, the question still remains of how the redox state of cytochrome c_6 can affect the stability of the transient complexes with its two partners so as to facilitate complex dissociation and turnover (34).

The Interaction of Cytochrome c_6 with PSI Trimers—The *in vivo* species of PSI embedded into the thylakoidal membrane is trimeric (19, 35). When cytochrome c_6 is not titrated with PSI monomers but with the physiological PSI trimers, most of the
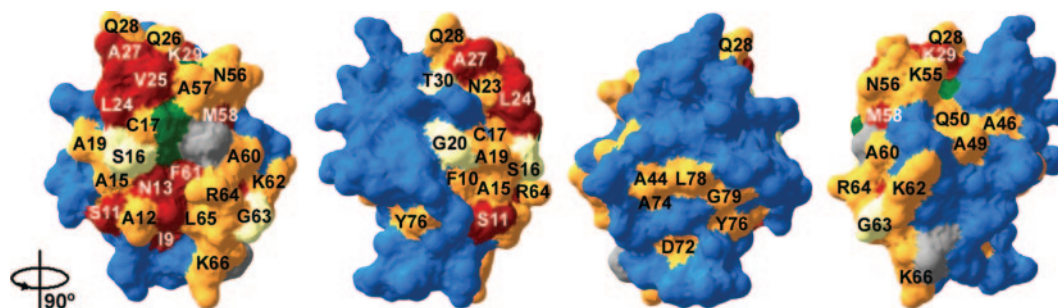
FIG. 4. **Map of *Nostoc* cytochrome c_6 interface upon binding to PSI.** Residues are colored according to their $\Delta\Delta\nu_{1/2\ \text{Binding}}$ and line width data for ^{15}N. The resonances that undergo the largest broadening (≥ 12 Hz) are *red*, and the signals with a significant line width over the detection limit but <12 Hz are *orange*. The limit of 12 Hz corresponds to a threshold value relative to the average plus 4-fold the standard deviation ($\Delta\Delta\nu_{1/2\ \text{Binding}} \geq \langle\Delta\Delta\nu_{1/2\ \text{Binding}}\rangle + 4S_{n-1}$). The residues broadened beyond the detection limit are *light yellow*, those with no line width perturbation are *blue*, prolines are *gray*, and the heme group is *green*.
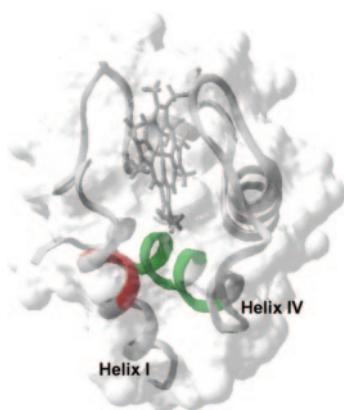

FIG. 5. **Line width changes ($\Delta\Delta\nu_{1/2\ \text{Binding}}$) displayed on the secondary structure of *Nostoc* cytochrome c_6.** *Red* indicates the residues of helix I with a line width perturbation ≥ 8 in ^{1}H and/or ^{15}N and direct interaction with PSI. The residues of helix IV with broadening ≥ 4 Hz and no direct interaction with PSI are in *green*. See "Results" for further details.
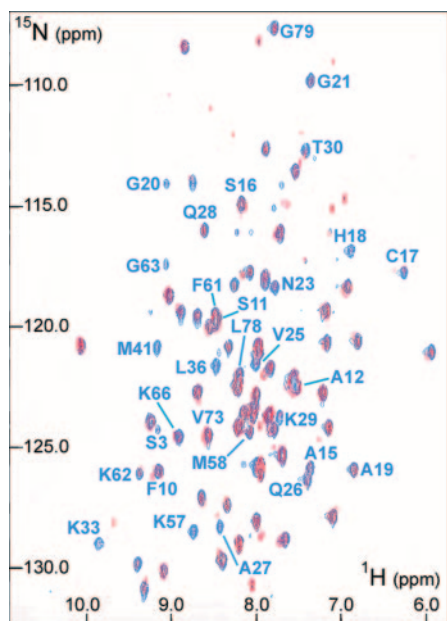

FIG. 6. **^{1}H-^{15}N TROSY spectra of *Nostoc* cytochrome c_6 before (*blue*) and after (*red*) the addition of PSI trimers.** The [PSI](μM)/[cytochrome c_6](μM) ratio was 38/208. The marked residues are those in which NMR signals undergo any perturbation upon binding to PSI.

cytochrome c_6 signals remain in the correlation spectrum (Fig. 6), with the exception of those being perturbed upon addition of PSI monomers. This finding could be due to the loss of sensi-

tivity inherent to high molecular weight systems because relaxation is not eliminated during the insensitive nuclei enhanced by polarization transfer steps in TROSY experiments (6). Thus, the signals that are specifically broadened in the presence of PSI monomers do not appear with PSI trimers. Most of the signals with PSI monomers are still visible with PSI trimers. This is so because we are observing the binding effects on the signals of free cytochrome c_6 rather than on the signals of the bound form, as is the case in the long-living complexes GroEL-GroES (8) and Hsp90-p53 (9).

REFERENCES

1. Diercks, T., Coles, M., and Kessler, H. (2001) *Curr. Opin. Struct. Biol.* **5,** 285–291
2. Zuiderweg, E. R. P. (2002) *Biochemistry* **41,** 1–7
3. Thompson, L. (2002) *Curr. Opin. Struct. Biol.* **12,** 661–669
4. Watts, A. (1999) *Curr. Opin. Biotechnol.* **10,** 48–53
5. Inooka, H., Ohtaki, T., Kitahara, O., Ikegami, T., Endo, S., Kitada, C., Ogi, K., Onda, H., Fujino, M., and Shirakawa, M. (2001) *Nat. Struct. Biol.* **8,** 161–165
6. Pervushin, K., Riek, R., Wider, G., and Wüthrich, K. (1997) *Proc. Natl. Acad. Sci. U. S. A.* **11,** 12366–12371
7. Tugarinov, V., Muhandiram, R., Ayed, A., and Kay, L. E. (2002) *J. Am. Chem. Soc.* **1,** 10025–10035
8. Flaux, J., Bertelsen, E. B., Horwich, A. L., and Wüthrich, K. (2002) *Nature* **418,** 207–211
9. Rüdiger, S., Freund, S. M. V., Vepritsev, D. B., and Fersht, A. (2002) *Proc. Natl. Acad. Sci. U. S. A.* **99,** 11085–11090
10. Fromme, P. (2003) *FEBS Lett.* **555,** 40–44
11. Golbeck, J. H. (2003) *Annu. Rev. Biophys. Biomol. Struct.* **32,** 237–256
12. Díaz-Quintana, A., Navarro, J. A., Hervás, M., Molina-Heredia, F. P., De la Cerda, B., and De la Rosa, M. A. (2003) *Photosynth. Res.* **75,** 97–110
13. Navarro, J. A., Hervás, M., Sun, J., De la Cerda, B., Chitnis, P. R., and De la Rosa, M. A. (2001) *Photosynth. Res.* **65,** 63–68
14. Sun, J., Wu, X., Hervás, M., Navarro, J. A., De la Rosa, M. A., and Chitnis P. R. (1999) *J. Biol. Chem.* **274,** 19048–19054
15. Molina-Heredia, F. P., Hervás, M., Navarro, J. A., and De la Rosa, M. A. (1998) *Biochem. Biophys. Res. Commun.* **243,** 302–306
16. Arslan, E., Schulz, H., Zufferey, R., Künzaler, P., and Thöny-Meyer, L. (1998) *Biochem. Biophys. Res. Commun.* **251,** 744–747
17. Crowley, P. B., Díaz-Quintana, A., Molina-Heredia, F. P., Nieto, P., Sutter, M., Haehnel, W., De la Rosa, M. A., and Ubbink, M. (2002) *J. Biol. Chem.* **277,** 48685–48689
18. Hervás, M., Ortega, J. M., Navarro, J. A., De la Rosa, M. A., and Bottin, H. (1994) *Biochim. Biophys. Acta* **1184,** 235–241
19. Ford, R. C. (1987) *Biochim. Biophys. Acta* **893,** 115–125
20. Mathis, P., and Sétif, P. (1981) *Isr. J. Chem.* **21,** 316–320
21. Arnon, D. I. (1949) *Plant Physiol.* **24,** 1–15
22. Hervás, M., Navarro, J. A., Díaz, A., Bottin, H., and De la Rosa, M. A. (1995) *Biochemistry* **34,** 11321–11326
23. Medina, M., Díaz, A., Hervás, M., Navarro, J. A., Gómez-Moreno, C., De la Rosa, M. A., and Tollin, G. (1993) *Eur. J. Biochem.* **213,** 1133–1138
24. Frazão, C., Soares, C. M., Carrondo, M. A., Poll, E., Daughter, Z., Wilson, K. S., Herrás, M., Navarro, J. A., De la Rosa, M. A., and Sheldrick, G. M. (1995) *Structure (Lond.)* **3,** 1159–1169
25. Kerfeld, C. A., Anwar, H. A., Interrante, R., Merchant, S., and Yeates, T. O. (1995) *J. Mol. Biol.* **250,** 627–647
26. Molina-Heredia, F. P., Díaz-Quintana, A., Hervás, M., Navarro, J. A., and De la Rosa, M. A. (1999) *J. Biol. Chem.* **274,** 33565–33570

27. De la Cerda, B., Díaz-Quintana, A., Navarro, J. A., Hervás, M., and De la Rosa, M. A. (1999) *J. Biol. Chem.* **274,** 13292–13297
28. Sahu, S. C., Bhuyan, A. K., Udgaonkar, J. B., and Hosur, R. V. (2000) *J. Biomol. NMR* **18,** 107–118
29. Stone, M. J. (2001) *Acc. Chem. Res.* **34,** 379–388
30. Goodman, J. L., Pagel, M. D., and Stone, M. J. (1999) *J. Mol. Biol.* **295,** 963–978
31. Crowley, P. B., and Ubbink, M. (2003) *Acc. Chem. Res.* **36,** 723–730
32. Hervás, M., Navarro, J. A., Díaz, A., and De la Rosa, M. A. (1996) *Biochemistry* **35,** 2693–2698
33. Danielsen, E., Scheller, H. V., Bauer, R., Hemmingsen, L., Bjerrum, M. J., and Hansson, Ò. (1999) *Biochemistry* **38,** 11531–11540
34. Bendall, D. S. (1996) in *Protein Electron Transfer* (Bendall, D. S., ed) pp. 43–68, Bios Scientific, Oxford
35. Jordan, P., Fromme, P., Witt, H. T., Klukas, O., Saenger, W., and Krauss, N. (2001) *Nature* **21,** 909–917